Sensors & Actuators: B. Chemical 321 (2020) 128500

Contents lists available at ScienceDirect

Sensors and Actuators B: Chemical

journal homepage: www.elsevier.com/locate/snb

Facile preparation of a hollow core-shell nanocomposite for the ultrasensitive sensing of glucose

Danfeng Jiang[a,b], Qingwen Zhang[a,b], Changshun Xu[a], Yuancai Ge[a,b], Liping Huang[a], Xueqian Ren[a], Yi Wang[a,b,*]

[a] School of Biomedical Engineering, School of Ophthalmology and Optometry, Eye Hospital, Wenzhou Medical University, Wenzhou, 325001, PR China
[b] Engineering Research Center of Clinical Functional Materials and Diagnosis & Treatment Devices of Zhejiang Province, Wenzhou Institute, University of Chinese Academy of Sciences, Wenzhou, 325001, PR China

ARTICLE INFO

Keywords:
Core-shell nanostructure
Hollow nanoflower
Ultrahigh sensitivity
Glucose sensor

ABSTRACT

A core-shell $Cu(OH)_2$@Au@$Co(OH)_2$ nanocomposite with hollow nano-flower morphology fabricated by a facile and non-surfactant template-engaged reaction was applied for highly sensitive detection of glucose. The prussian blue analogues (PBA) of core-shell nanocubes (CuFe@Au@CoFe) were synthesized as the template through the accurate control of the reaction rate. In this nanocubes, Au nanoparticles for accelerating electron transfer rate were reduced at the interface of CoFe (core) and CuFe (shell) to improve their conductivity. These nanocubes were then etched controllably to form three-dimensional hollow nanoflowers stacked by nanosheets. It provided abundant electrode-electrolyte channels and high surface areas for OH^- and glucoses adsorption and the following reactions. Due to the sandwich structure and synergic effect of the nanomaterials, the as-prepared sensors exhibited an ultrahigh sensitivity of 3427 $\mu A\ mM^{-1}\ cm^{-2}$ for glucose detection, as well as a wide linear range of 0.001–5.2 mM with a low detection limit of 0.5 μM. In addition, the $Cu(OH)_2$@Au@$Co(OH)_2$ nanocomposite showed long-term stability and good reproducibility for glucose detection in serum with comparable results as measured with commercial glucometer. We believe the nanocomposite provided a good candidate for glucometer in future clinical applications.

1. Introduction

The increasing attentions have been paid to diabetes, because it is the cause of many severe chronic diseases, such as blindness, kidney impairment and peripheral neuropathy [1,2]. According to the report from the World Health Organization, the number of diabetics will reach to 578 million by 2030 [3]. Monitoring the glucose level is the unique and effective way to maintain their health [4,5]. Among a great variety of detection methods, electrochemical glucose sensors receive extensive interests due to the attractive properties of low cost, simple operation, rapid response and ease of miniaturization [6,7]. Nevertheless, current detection methods based on electrochemical glucose sensors (glucometers) mainly rely on the activity of glucose oxidase which may be denatured under inappropriate storage [8,9]. Pursuing a highly efficient electrochemical sensor with strong stability is always a worthy goal. To reach the aim, considerable efforts have been conducted to explore novel electrocatalytic materials with highly enzyme-mimic activity and long-term stability.

Up to date, numerous metallic materials, considered as the enzyme-mimic candidates (such as CuO, Cu_3N, Co_3O4, Co_3N, NiO, $Cu(OH)_2$, $Co(OH)_2$, $Ni(OH)_2$) [10–17], have been utilized in the preparation of non-enzymatic sensors, due to their ability to oxidize glucose. However, catalytic materials with high sensitivity, good environmental adaptability and excellent stability especially applied in real samples are still under development [18,19]. Instead of single component materials, composite nanomaterials may offer improved performance due to their synergic effects in catalytic activity, conductivity and active areas. For instance, nanocomposites such as CeO_2@CuO, TiO_2/Co_3O_4, ZnO-CuO and nickel-cobalt double layered hydroxide [11,20–22] have shown high sensitivity and stability for glucose detection. In addition, $Fe(OH)_3$ and $Cu(OH)_2$ nanowires were designed to core-shell nanostructure for the improvement of the intrinsic activity and the electrochemical surface areas were also larger than their previous work [23]. The combinations of metal hydroxides with well-designed nanostructure offer large specific surface, high redox activity and chemical stability [24,25]. However, the deficiency of high conductivity of such metal

* Corresponding author at: School of Biomedical Engineering, School of Ophthalmology and Optometry, Eye Hospital, Wenzhou Medical University, Wenzhou, 325001, PR China.
E-mail address: wangyi@wibe.ac.cn (Y. Wang).

https://doi.org/10.1016/j.snb.2020.128500
Received 25 March 2020; Received in revised form 17 June 2020; Accepted 21 June 2020
Available online 23 June 2020

hydroxides nanocomposites limits their further applications. The feature of semiconductive materials typically postpones the electron transfer to the electrode surface upon glucose catalysis [26]. Consequently, nanomaterials with strong conductivity, especially Au nanoparticles, were often doped into composite nanomaterials to facilitate the electron transfer [27–29]. Under the synergies of bimetallic atoms and conducting nanoparticles, a nanocomposite containing $Cu(OH)_2$, $Co(OH)_2$ and Au may offer enhanced catalytic activity.

Along with the development of advanced synthetic technology and the deep comprehension of micro/nanostructural formation mechanism, the contribution of geometric configuration to sensing performance was gradually revealed [30–33]. The preparation of a suitable nanostructure with spatial configuration and interfacial distribution with multiple materials to achieve excellent sensing performance is still challenging. Various novel nanostructures were continuously developed for the preparation of high-active materials with abundant active sites, strong electrocatalytic property and excellent stability [34,35]. Among all the nanostructures, the construction of core-shell and hollow structure was considered as two of the promising strategies [36–39]. For the core-shell structure, their catalytic activity can be effectively improved via the regulation of their shell shape and shell thickness. Hollow and porous structure played a paramount role in respect to their electric transport efficiency. Interior cavity provided high surface-area-to-volume ratio for effective molecules reaction and electron diffusion, which is beneficial for highly catalytic activity [40]. The interior void space provided also improved reusability in applications due to the avoidance of destructive volume expansion and the alleviation of structure stress strain [41]. Therefore, in order to obtain the desirable functionalities, integrating effectively different nanomaterials/structures to form a hollow core-shell structure is an appealing strategy.

Herein, the hollow core-shell structural nanocomposites of $Cu(OH)_2$@Au@$Co(OH)_2$ were prepared by a facile and non-surfactant template-engaged reaction for glucose catalysis and monitoring. As shown in Fig. 1, a dense thin Au layer served as a conductive layer was firstly reduced on the surface of $Co_3[Fe(CN)_6]_2$ (CoFe) core layer. After that, a shell layer of $Cu_3[Fe(CN)_6]_2$ (CuFe) was grown on the Au surface along with the structure changes from the truncated cubes to well-defined cubes. Finally, a hollow core-shell nanocomposite with highly structural complexity was formed under an alkaline etching process. Interestingly, through the regulation of the etching concentration and shell thickness, different nanostructures with high surface areas were generated such as nanowire networks, nanowire flowers and nanosheet flowers. Due to the synergies between the catalysis from bimetallic atoms and the conductivity from Au nanoparticles, the as-prepared sensor exhibited outstanding electrocatalytic activity towards glucose with ultrahigh sensitivity, long-term stability and high accuracy for glucose detection in serum.

2. Experiments

2.1. Reagents and apparatus

Cobalt (II) chloride ($CoCl_2$), cupric chloride ($CuCl_2$), gold (III) chloride trihydrate ($HAuCl_4$•$3H_2O$), sodium hydroxide (NaOH), glucose, uric acid (UA), dopamine (DA), fructose (Fru), lactose (Lac) and sodium chloride (NaCl) were purchased from Shanghai Macklin Biochemical Co., Ltd. Potassium ferricyanide ($K_3Fe(CN)_6$) and ascorbic acid (AA) were received from Shanghai Aladdin Bio-Chem Technology Co., Ltd. Ethylalcohol was bought from Anhui Ante Food Co., Ltd. Rabbit serum was obtained from Beijing Huaaokean Technology Co., Ltd. Au, Pt and Ag/AgCl (saturated KCl) electrodes were received from Shanghai Chuxi Industry Co., Ltd. Glucometer was purchased from ACON Laboratories, Inc.

Field emission scanning electron microscope (FESEM, Hitachi, SU8010, working potential: 5 KV, working current: 10 μA) and Field emission transmission electron microscopy (FETEM, F200S, working potential: 200 KV) were used to investigate the morphology of the prepared materials. Fourier-transform infrared (FTIR, Tensor II, USA, wavelength range: 400–4000 cm^{-1}), Raman spectrometer (Renishaw, InVia Qontor, England, laser wavelength: 633 nm, laser power 1%) and X-ray diffractometer (D/MAX 2500 V/PC, working potential: 40 KV, working current: 15 mA, scan range: $5-60^0$, scan rate: 15°/min) with a Cu-Ka radiation (0.15419 nm) were respectively utilized to character the components and structure of the nanocomposites. X-ray

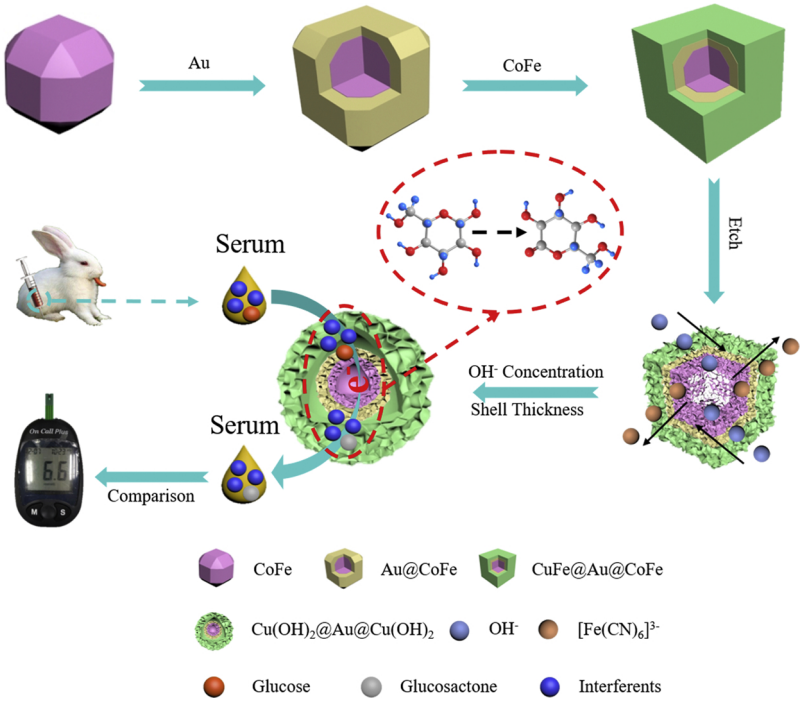

Fig. 1. Schematic illustration for the preparation and application of hollow core-shell $Cu(OH)_2$@Au@$Co(OH)_2$ nanocomposites for glucose monitoring in serum, which was compared with that measured by a commercial glucometer.

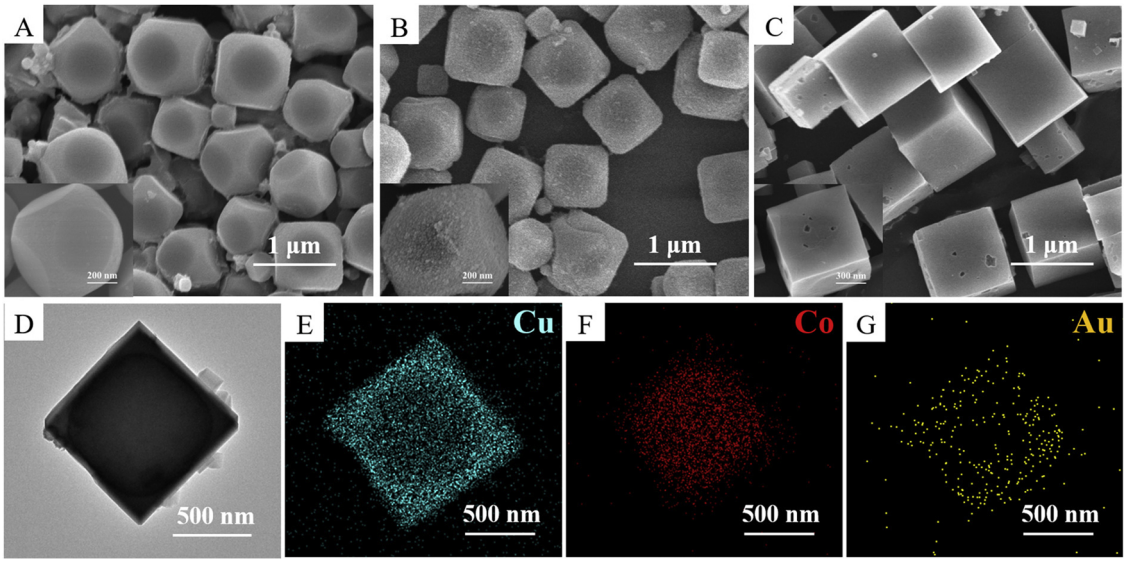

Fig. 2. SEM images of (A) CoFe, (B) Au@CoFe and (C) CuFe@Au@CoFe. (D) The TEM image of a CuFe@Au@CoFe nanoparticle. The elements mapping images of (E) Cu, (F) Co and (G) Au, respectively.

photoelectron spectrometer (ESCALABMKLL) was applied to investigate elements valence state. The Brunauer-Emmett-Teller (BET) surface area and porosity analyzer (ASAP 2460, Micrometritics, analysis gas: nitrogen, outgas time: 12.0 h) was utilized to measure the specific surface areas of the nanostructured materials. Plasma emission spectrometer (Agilent, ICPOES730) was used to determine the element content of metal in the composite.

2.2. The precursor fabrication of core-shell structural CuFe@Au@CoFe

Firstly, based on a chemical reaction of Co^{2+} and $[Fe(CN)_6]^{3-}$, a mixture of 10 mM $CoCl_2$ and 10 mM $HAuCl_4$ was prepared to react with $K_3Fe(CN)_6$ for the formation of truncated cubic CoFe (Core) with the assistance of syringe pump. Then, excess 10 mM AA was slowly added to reduce $AuCl_4$- on the core surface thanks to the electrostatic interaction of $AuCl_4$- with Co^{2+} (Fig. 1). After that, Au@CoFe was washed with water by three times at 6000 rpm centrifugation rate, and redistributed in 20 mL water. Then, 10 mM $CuCl_2$ and 10 mM $K_3Fe(CN)_6$ was injected into the above solution at a slow rate (100 μL/min) to form CuFe shell layer. Finally, the formed core-shell composite was dissolved in 20 mL ethanol after centrifugation for three times. Shell thickness was adjusted by changing the added volume of $CuCl_2$ and $K_3Fe(CN)_6$.

As control, CoFe and CuFe nanoparticles were synthesized by the chemical reaction of 10 mM $CoCl_2$ with 10 mM $K_3Fe(CN)_6$ and 10 mM $CuCl_2$ with 10 mM $K_3Fe(CN)_6$, respectively. The synthesize of Au@CuFe was similar to above method for the synthesis of Au@CoFe by replacing $CoCl_2$ with $CuCl_2$. Au nanoparticles with diameter around 10 nm were formed by using the 10 mM AA to reduce $HAuCl_4$ as reported elsewhere [25].

2.3. The construction of hollow core-shell $Cu(OH)_2$@Au@$Co(OH)_2$ based sensor

40 mL of 0.6 M NaOH was added into the above 20 mL ethanol solution containing CuFe@Au@CoFe to form the $Cu(OH)_2$@Au@$Co(OH)_2$ structure based on the alkaline etching reaction as shown in Eqs. 1 and 2. After hand shaking for 5 min, the mixed solution was sonicated for 15 min. Note that in order to investigate the morphologies variations, different concentrations of NaOH (from 0.2 M to 0.8 M) were used during the etching process. The as-prepared product was heated in oven at 60 °C for 6 h. The sensors were fabricated by dropping cast of 10 μL $Cu(OH)_2$@Au@$Co(OH)_2$ aqueous solution (2 mg/mL) on the Au electrodes and dried at room temperature before usage. The preparations of $Cu(OH)_2$, $Co(OH)_2$, Au@$Cu(OH)_2$ and Au@$Co(OH)_2$ particles were obtained by using the 0.6 M NaOH to etch the above prepared CuFe, CoFe, Au@CuFe and Au@CoFe particles.

$$6OH^- + Cu_3[Fe(CN)_6]_2 = 3Cu(OH)_2 + 2[Fe(CN)_6]^{3-} \quad (1)$$

$$6OH^- + Co_3[Fe(CN)_6]_2 = 3Co(OH)_2 + 2[Fe(CN)_6]^{3-} \quad (2)$$

2.4. Electrochemical measurement

All electrochemical tests were conducted on electrochemical workstation of Shanghai Chenhua Instrument Co.Ltd (CHI 660E). Cyclic voltammetry (CV) and chronoamperometry tests were performed in a 0.5 M NaOH electrolyte. I–T curves were obtained by the successive addition of quantitative glucose solution into the electrolyte, while serum sample detection was conducted by adding 400 μL serum into 40 mL 0.5 M NaOH solution at 0.5 V working potential. Electrochemical impedance spectroscopy (EIS) was performed in a hybrid solution of 5 mM $[Fe(CN)_6]^{4-/3-}$ (1:1) and 0.1 M KCl. Its frequency range was set from 0.1 Hz to 1000 kHz with the initial test voltage of 0 V and amplitude of 5 mV. An Ag/AgCl (saturated KCl) electrode and a Pt wire were respectively utilized as the reference electrode and the counter electrode.

3. Result and discussion

3.1. The preparation and characterization of precursor

To synthesize hollow core-shell structural nanocomposites, a template-engaged reaction based on Prussian blue analogues (PBA) is adopted [42,43]. It is important to obtain regular skeleton frame structure of PBA, which dominates the morphology of $Cu(OH)_2$ and $Co(OH)_2$. Owing to the rapid reaction rate of $[Fe(CN)_6]^{3-}$, Cu^{2+} and Co^{2+}, PBA with regular cubic structure is usually hard to be formed by tradition chemical synthesis without well-control of the crystal growing rate [29,44]. We however precisely controlled the reactant amount through syringe pump injection to form the truncated cubic CoFe as shown in Fig. 2A. After that, Au nanoparticles were reduced uniformly on its surface when AA was added to generate the truncated cubic Au@CoFe particles (Fig. 2B). Interestingly, after the deposition of CuFe layer on the surface of Au@CoFe, the sharp-edge cubes were obtained

as shown in Fig. 2C. The change in geometry caused by core-shell structure had not been reported previously. Due to the slowing growth rate, the CuFe and Au layers were mainly grown around the core rather than formed self-nucleation [45]. The TEM image and element mapping (Fig. 2D–F) were used to confirm the structure and the distribution of characteristic elements. Apparently, the Co atoms were wrapped by Cu, and in between the Au atoms were randomly distributed, indicating the successful formation of CuFe@Au@CoFe sandwich structure. In addition, the mass ratio of element in the composites for Cu, Au and Co was estimated as 1.7:1:1.06, which was comparable with the results measured by ICP as 25.9 % (Cu), 12.9 % (Au) and 12.7 % (Co) in mass fraction. Note that the element mapping measured by TEM only represented the single particle, while ICP measurement gave the bulk information of the composites which avoided the component variations among the particles.

The XRD diffraction spectroscopy was utilized to analyze the synthetic process of the nanocomposite. From Fig. S1A, the sharp peaks of CoFe at 2θ value located at 17.3°, 24.6°, 34.9°, 39.2°, 43.0°, 50.1°, 53.4° and 56.5° respectively represented the crystalline plane of (200), (220), (400), (420), (422), (440), (600) and (620), illustrating excellent crystal phase purity [46,47]. For CuFe@CoFe composite, the characteristic peaks of CuFe were adjacent to CoFe, located at 17.6°, 25.1°, 35.8°, 40.1°, 44.1°, 51.4°, 54.8° and 58.2°, respectively. Furthermore, Au peaks of (111) and (200) planes were evidently found in the CuFe@Au@CoFe nanocomposites (Fig. S1A) [48]. The phenomenon indicated CuFe, Au and CoFe were successfully synthesized by the simple non-surfactant method. Similarly, FTIR spectroscopy was applied to further confirm the composition of nanocomposite by functional group. In different synthetic progresses, two strong adsorption peaks were always observed at 2102 cm^{-1} and 2160 cm^{-1}, which corresponded to the stretching vibration band of −CN− group of PBA (Fig. S1B) [49,50]. It indicated that the non-surfactant method for core-shell preparation had negligible impact on the PBA crystal structure.

3.2. The morphology regulation and performance optimization of $Cu(OH)_2$@Au@$Co(OH)_2$ based electrode

To obtain the nanocomposite of $Cu(OH)_2$@Au@$Co(OH)_2$ with glucose oxidizing capability, NaOH was selected to etch the synthesized precursor of CuFe@Au@CoFe, based on a simple ion exchange reaction as shown in Eqs. 1 and 2. At the initial stage of etching, a thin metal hydroxide layer was grown on PBA surface via the chemical reaction of Cu^{2+} from PBA with OH^- in alkaline solution. As the ion-exchange reaction proceeded, OH^- flowed into the crystal interior and the displaced $[Fe(CN)_6]^{3-}$ diffused out to the solution. When continuous OH- were provided, the Co^{2+} from the core would migrate outwards to form a new $Co(OH)_2$ shell. Hence, sufficient OH- could induce the formation of hollow multishell configuration. Considering the different reaction kinetics caused by diverse OH^- concentrations, we investigated the effect of alkaline concentration to the morphology of $Cu(OH)_2$@Au@Co$(OH)_2$ nanocomposite. From Fig. 3A–D, the morphology of four different nanostructured $Cu(OH)_2$@Au@$Co(OH)_2$ were exhibited. At a low concentration of NaOH solution (0.2 M), numerous $Cu(OH)_2$ nanowires were spread over the $Co(OH)_2$ hollow crystal and formed a network structure on the particle surface. Interestingly, with increasing the pH value of the reaction solution, nanowires were gradually converted to nanosheets. Furthermore, in the case of 0.6 M NaOH, these nanosheets were orderly assembled to form a porous nanosphere structure, providing abundant electrode-electrolyte channels for glucose catalysis. However, once the concentration was increased up to 0.8 M NaOH, nanowires or nanosheets were both disappeared with the presence of small nanoparticles. This may be because that high OH^- concentration tremendously boosted the reaction rate and the ion diffusion rate, therefore large amount of nucleus were formed rapidly and converted to nanoparticles rather than nanosheets. On the basis of the above etching phenomenon, it could be summarized that the complexed nanostructure could be controlled by the etchant concentration.

Raman and FTIR characterizations were performed to verify the etching method. In Fig. 3E, the Raman scattering peak at 2158 cm^{-1}, ascribed to the stretching vibration of −CN− in PBA [51,52], was disappeared after PBA was converted to metal hydroxides. Similar phenomenon was revealed in FTIR spectra (Fig. 3F) that the stretching adsorption peaks of -CN- at 2102 and 2160 cm^{-1} in the nanocomposite of $Cu(OH)_2$@Au@$Co(OH)_2$ were both disappeared. In Fig. S2A, the XRD measurement also showed obvious elimination of peaks for CuFe and CoFe but presence of peaks at 19.4°, 35.9° 38.4° and 44.6°, corresponding to the (001) crystalline plane of $Co(OH)_2$, (111) crystalline plane of $Cu(OH)_2$, the (111) and (200) crystalline plane of Au, respectively [29,53,54]. XPS measurement was applied to investigate the chemical compositions after the generation of Au and hydroxides. In Fig. S2B, two Au 4f peaks located at 83.9° (Au $4f^{7/2}$) and 87.6° (Au $4f^{5/2}$) represented the existence of metallic gold Au (0). For cobalt and copper element, their oxidation state remained unchanged as revealed in Fig. S2C and D when Au nanoparticles were reduced in composites, demonstrating the limited impact of the reduction progress on their valence state. Moreover, the location of two main Co 2p peaks (780.5 eV Co $2p^{3/2}$, 795.7 eV Co $2p^{1/2}$) and the location of two Cu 2p peaks (933.5 eV Co $2p^{3/2}$, 953.5 eV Co $2p^{1/2}$) respectively illustrated the existence of Co^{2+} and Cu^{2+} in $Co(OH)_2$ and $Cu(OH)_2$ phase [55,56]. The results confirmed that there was no side reaction during the etching process.

As mentioned previously, different nanostructured materials possessed diverse catalytic activities. To obtain the optimal nanostructures for catalysis, the electrochemical behaviors of four $Cu(OH)_2$@Au@Co$(OH)_2$ nanocomposites fabricated at different NaOH concentrations (0.2 M to 0.8 M) were respectively measured by CV and chronoamperometry technologies in the electrolyte of 0.5 M NaOH. Compared with other concentrations of NaOH, the nanocomposite obtained at 0.6 M NaOH showed the highest current intensity of redox peaks, representing the best electrocatalytic activity (Fig. 4A). It was mainly because that the three-dimensional porous morphology assembled by nanosheets (as shown in Fig. 3C) supplied abundant electrolyte-accessible channels, which were beneficial to the generation of peroxide. The $Cu(OH)_2$@Au@$Co(OH)_2$ composite was then applied for studying the CV responses to various concentrations of glucose (0–1.2 mM). The CV results showed significant increase of oxidization peak intensity and the decrease of reduction peaks upon increasing the concentration of glucose (Fig. 4B). The limiting mechanism of the electrochemical reaction on the $Cu(OH)_2$@Au@$Co(OH)_2$ based electrode for glucose catalysis was investigated as shown in Fig. S3. The linear proportional of the redox peaks vs. the square root of scan rate (40 to 240 mV s^{-1}) indicated a diffusion-control electrochemical reaction process (Fig. S3) [6,57].

To investigate the sensitivity of $Cu(OH)_2$@Au@$Co(OH)_2$ composites to glucose at different working potentials, the chronoamperometry measurements were carried out at 0.4 V, 0.5 V and 0.6 V respectively, upon the successive addition of 0.1 mM glucose into 0.5 M NaOH solution (Fig. S4). Note that the three voltages were selected according to the current changes as measured in the CV measurement (Fig. 4B). The results in Fig. S4 indicated that the current response at working potential of 0.5 V provided the highest current response upon the injection of the same concentration of glucose into the reactive cell. Therefore, 0.5 V was applied for the subsequent chronoamperometry tests. In addition, the electrocatalytic activity of different $Cu(OH)_2$@Au@$Co(OH)_2$ composites to glucose were also investigated similarly with the chronoamperometry measurements. In Fig. 4C, steady current steps with rapid response were observed, and the largest current response was presented for the nanocomposite with nanosheets structures fabricated under 0.6 M NaOH etching solution. This nanosheets structural electrode showed highest sensitivity of 3427 μA mM^{-1} cm^{-2} to glucose catalysis, which was nearly double of that measured on nanocomposites prepared under 0.4 and 0.8 M NaOH (Fig. 4D). The results were in

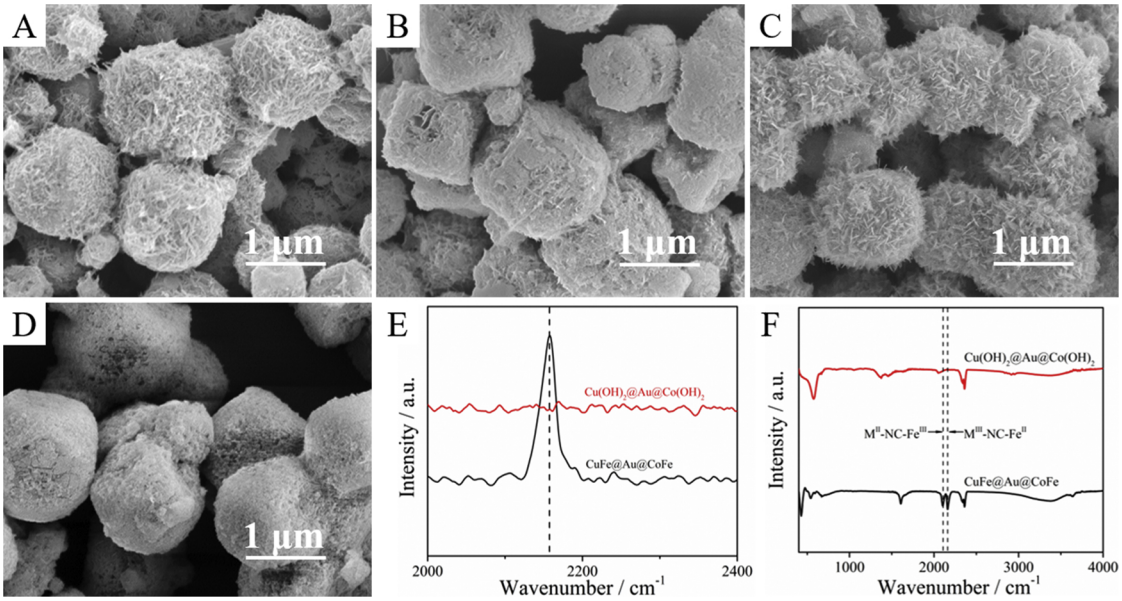

Fig. 3. SEM images of $Cu(OH)_2$@Au@$Co(OH)_2$ fabricated at different NaOH concentrations: (A) 0.2 M, (B) 0.4 M, (C) 0.6 M and (D) 0.8 M. (E) The Raman and (F) FTIR spectra comparison of CuFe@Au@CoFe and $Cu(OH)_2$@Au@$Co(OH)_2$ nanoparticles.

accordance with that measured in CV (Fig. 4A). The generated three-dimensional nanoporous morphology was responsible for their high sensitivity. Based on the Eqs. 3–7 [13,58], it could be learned that more peroxides were produced due to the increase of effective specific surface areas resulted from the outer stacked nanosheets and interior hollow cavity. The BET areas of four different nanostructures were measured with the typical N_2 adsorption-desorption isotherms as shown in Fig. S5. Meanwhile, as shown in Fig. 4D, the composite obtained at 0.6 M NaOH showed the largest specific surface areas, reaching to 210.5 $m^2 g^{-1}$. Moreover, the specific surface areas of four different nanostructured composites (182.4 $m^2 g^{-1}$, 102.9 $m^2 g^{-1}$, 210.5 $m^2 g^{-1}$ and 107.9 $m^2 g^{-1}$) were larger than the composites before etching (76.2 $m^2 g^{-1}$, i.e. the CuFe@Au@CoFe nanostructure as indicated in Fig. 2C). Abundant catalytic sites on the nanocomposite could be easily accessible for glucose molecules. Consequently, based on the results of CV, chronoamperometry and BET tests, 0.6 M NaOH was considered as the optimal etching concentration.

$$Cu(OH)_2 + OH^- \rightarrow CuOOH + H_2O + e^- \quad (3)$$

$$CuOOH + glucose \rightarrow Cu(OH)_2 + gluconolactone \quad (4)$$

$$Co(OH)_2 + OH^- \rightarrow CoOOH + H_2O + e^- \quad (5)$$

$$CoOOH + OH^- \rightarrow CoO_2 + H_2O + e^- \quad (6)$$

$$2CoO_2 + glucose \rightarrow 2CoOOH + gluconolactone \quad (7)$$

The structure of PBA precursor determined the exhibited morphology and structure of $Cu(OH)_2$@Au@$Co(OH)_2$ composite. Through

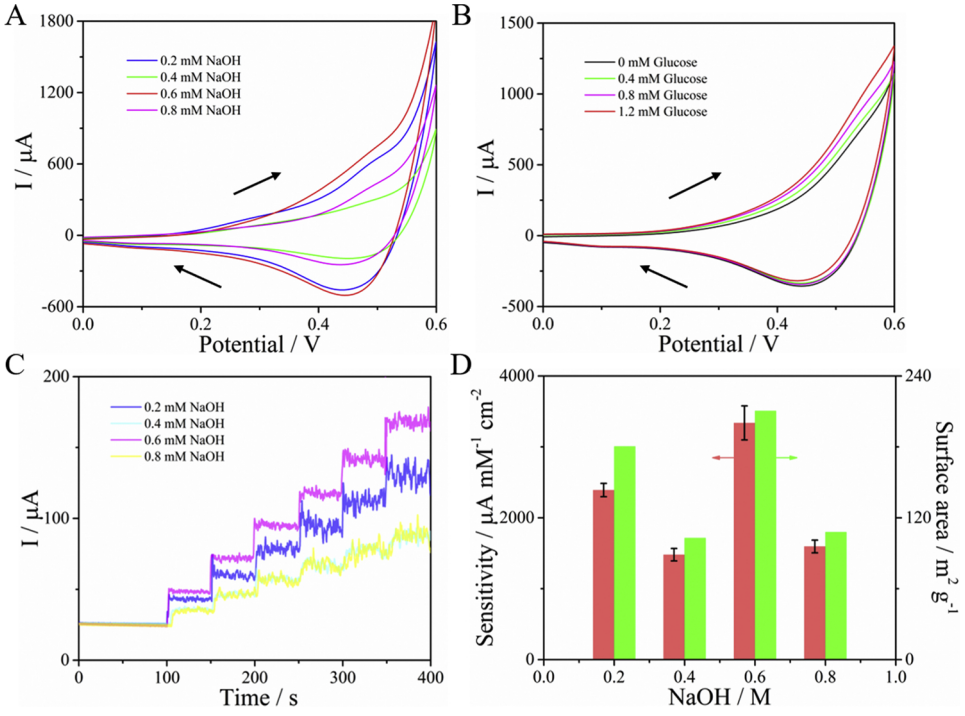

Fig. 4. (A) CV measurements carried out in 0.5 M NaOH solution, for Au electrodes modified with different $Cu(OH)_2$@Au@$Co(OH)_2$ composites prepared under 0.2 M, 0.4 M, 0.6 M and 0.8 M NaOH solution with the same 0.4 mM $CuCl_2$, respectively. (B) CV responses of $Cu(OH)_2$@Au@$Co(OH)_2$ prepared at 0.6 M NaOH and 0.5 mM $CuCl_2$ measured in different concentrations of glucose (0-1.2 mM) with 0.5 M NaOH solution. (C) The chronoamperometry measurements upon the successive injection of 0.1 mM glucose into 0.5 M NaOH solution for Au electrodes modified with different $Cu(OH)_2$@Au@$Co(OH)_2$ composites fabricated under 0.2 M, 0.4 M, 0.6 M and 0.8 M NaOH, respectively. (D) The sensitivity to glucose detection applied on electrodes modified with different nanocomposites corresponding to that in Fig. 4C and BET areas of different nanocomposites.

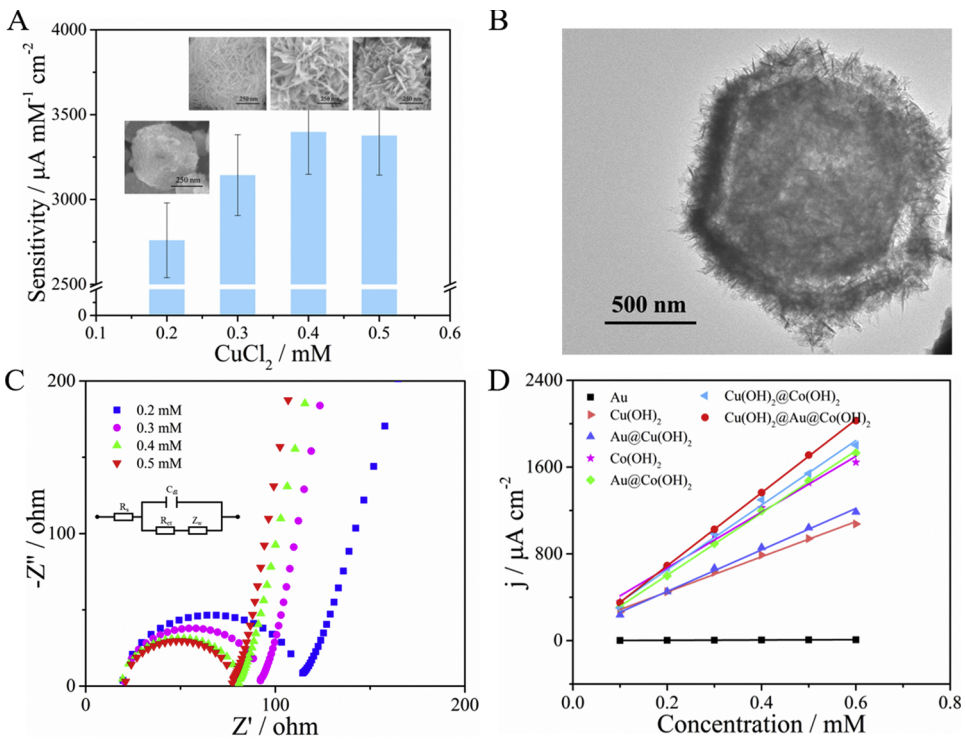

Fig. 5. (A) The glucose sensitivity of electrodes modified with four different morphologies of nanomaterials fabricated by adding different concentrations of $CuCl_2$ (0.2 mM, 0.3 mM, 0.4 mM and 0.5 mM). Inset: the SEM images presented the particles morphology obtained under the corresponding $CuCl_2$ concentration. (B) The TEM image of $Cu(OH)_2$@Au@$Co(OH)_2$ nanocomposite fabricated under 0.5 mM $CuCl_2$. (C) The EIS characterization of Cu $(OH)_2$@Au@$Co(OH)_2$ modified electrodes prepared at four different concentrations of $CuCl_2$ (0.2 mM, 0.3 mM, 0.4 mM and 0.5 mM). Inset: the equivalent circuit used to plot the resistances of the electrodes. (D) The current response of electrodes modified with different nanocomposites to various concentration of glucose, including Au, $Cu(OH)_2$, Au@$Cu(OH)_2$, $Co(OH)_2$, Au@$Co(OH)_2$, Cu$(OH)_2$@$Co(OH)_2$, and Cu$(OH)_2$@Au@$Co(OH)_2$ particles.

the regulation of etching concentration, core-shell structure with three-dimensional porous morphology can be obtained, which provided high specific surface areas for glucose accessibility. In addition, the amount of Cu and Co element in the nanocomposites also affected the sensor sensitivity due to their involvement in the catalytic reaction via the conversation of Cu^{2+} to Cu^{3+} and Co^{2+} to Co^{3+}. For instance, the effect of added $CuCl_2$ to the sensor activity was investigated as shown in Fig. 5A. When 0.4 mM or 0.5 mM $CuCl_2$ was added to the reaction solution, $Cu(OH)_2$@Au@$Co(OH)_2$ based electrode exhibited an ultrahigh sensitivity to glucose, reaching to 3427 μA mM^{-1} cm^{-2}. In a low concentration of 0.2 mM $CuCl_2$, the cubic-shape nanoparticles with relatively poor rough surface was achieved (inset in Fig. 5A), along with low sensitivity to glucose catalysis (2760 μA mM^{-1} cm^{-2}). At the presence of 0.3 mM $CuCl_2$, the nanoparticles with a network morphology stacked by nanowires was obtained on the surface (inset in Fig. 5A). Interestingly, the composites covered with obvious nanowires and nanosheets structure were formed after increasing the amount of $CuCl_2$ to 0.4 or 0.5 mM. The thick shell caused by the high concentration of $CuCl_2$ may hinder the etching process which induced the formation of nanoflower morphology. The TEM image of the nanoflower was shown in Fig. 5B and an obvious hollow core-shell structure was presented. Therefore, both 0.4 and 0.5 mM $CuCl_2$ could be used for the fabrication of the nanocomposites. The EIS was used to further investigate the charge transfer resistance (R_{ct}) at electrode surface and the R_{ct} was obtained according to the classical Randles circuit (Fig. 5C inset). The test was conducted in a 5 mM $[Fe(CN)_6]^{4-/3-}$ solution containing 0.1 M KCl with a frequency range from 0.1 to 10^6 Hz. For electrodes fabricated at different $CuCl_2$ concentrations, the values of R_{ct} were fitted respectively as 114.4 (0.2 mM $CuCl_2$), 92.7 (0.3 mM $CuCl_2$), 79.9 (0.4 mM $CuCl_2$) and 78.3 Ω (0.5 mM $CuCl_2$). It could be obviously found that the R_{ct} of nanocomposite-modified electrodes gradually decreased from 114.4 to 78.3 Ω with increasing the amount of $CuCl_2$. The electrode modified with nanocomposite fabricated under 0.4 mM $CuCl_2$ was similar to that for 0.5 mM $CuCl_2$. Compared with other morphologies, these two nanoflower morphologies offered the highest sensitivity for glucose detection indicating the ample paths for electron transfer and effectively low diffusion resistance.

Furthermore, to further improve the electron transfer efficiency, Au nanoparticles were introduced and the structure of nanomaterial was optimized. In Fig. 5D, the slope of the calibration curves for glucose detection represented the catalytic ability to glucose. Due to the strong electrocatalysis originated from core-shell bimetallic structure, the Cu $(OH)_2$@$Co(OH)_2$ composites showed 259.1, 2.1 and 1.3 times higher sensitivity for glucose detection as compared with the Au, $Cu(OH)_2$ and $Co(OH)_2$ nanoparticles, respectively (Fig. 5D). Furthermore, the particles after doped with Au nanoparticles, i.e. Au@$Cu(OH)_2$, Au@$Co(OH)_2$ and $Cu(OH)_2$@Au@$Co(OH)_2$, showed improved sensitivity as compared with their counterparts, i.e. $Cu(OH)_2$, $Co(OH)_2$ and $Cu(OH)_2$@$Co(OH)_2$, respectively. It was because that Au nanoparticles located at the interface of $Cu(OH)_2$ and $Co(OH)_2$ facilitated remarkably the electron transfer. The comparisons proved that the sandwich structure and Au nanoparticles significantly boosted the electrochemical activity.

3.3. The electrochemical behaviors of the as-prepared sensors

The amperometric responses of the as-prepared sensor based on Cu $(OH)_2$@Au@$Co(OH)_2$ composites to different concentrations (1 μM, 10 μM, 100 μM, 500 μM, 1 mM and 2 mM) of glucose were recorded in Fig. 6A. Along with the successive addition of glucose, the steady current steps with sensitive electric response (≤5 s) were observed and it could last for a while until next injection. Moreover, the current value maintained a staircase increase upon increasing the glucose concentration. As exhibited in the calibration curve of Fig. 6B, the current density was proportional to glucose concentration from 0.001 to 5.2 mM. The detection limit was further investigated with low concentrations of glucose (from 0.1 to 1 μM) as shown in Fig. S6. The results showed the current response to 0.5 μM glucose (ΔI = 0.13 μA) was about 8 times higher than the noise level (i.e. the standard deviation, N = 0.016 μA), while the response for 0.1 μM glucose (ΔI = 0.03 μA) was smaller than three times of noise level. Therefore, a low detection limit of 0.5 μM was achieved in the sensor system. Compared with other currently reported glucose sensors in Table S1, the as-prepared sensor revealed a competitive superior in sensitivity and linear range of detection.

In addition, before the real-sample applications, the selectivity of the sensor was investigated by injecting different interferents such as

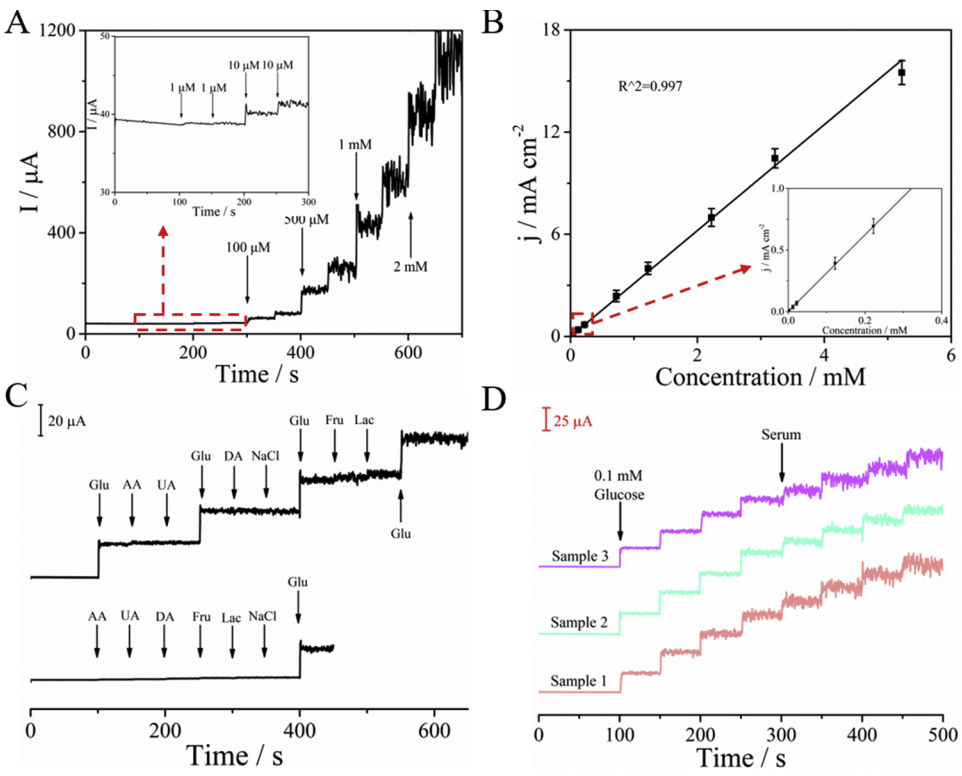

Fig. 6. (A) The current response of the as-prepared sensors to different concentrations (1 μM, 10 μM, 100 μM, 500 μM, 1 mM and 2 mM) of glucose at working potential of 0.5 V. (B) The calibration curve for the detection of glucose. (C) The selectivity test for the current response of the as-prepared sensors to glucose as compared with the interferents such UA, AA, DA, fructose and lactose. (D) The amperometric responses of the as-prepared sensor to glucose upon the injection of 4 μL (1 M) glucose at the first 4 injections and 400 μL undiluted rabbit serum at the following injections into total of 40 mL (0.5 M NaOH) electrolyte solution.

UA, AA, DA, fructose, lactose and NaCl into the reaction cell. The sensor responses to the following interferents such as 0.01 mM UA, AA, DA, fructose, lactose and 1 mM NaCl were compared with that for 0.1 mM glucose. Note that the concentrations of the interferents were chosen due to the fact that the UA, AA, DA, fructose and lactose in serum are at least 10-fold lower than that of glucose. As shown in Fig. 6C, the injection of interferents showed negligible current variations as compared to the response for glucose. The change in current with the addition of substances indicated an excellent selectivity to glucose for the prepared sensor. The reproducibility was evaluated by the measurement of six independent sensors fabricated at the same condition. In Fig. S7, the relative standard deviation (RSD) of the sensitivity to glucose was calculated as 5.2 %, implying good reproducibility of the sensors. The long-term stability of the as-prepared sensors was measured repeatedly every five days over 30 days. Note that the sensor was usually stored at 4 °C in refrigerator before usage. The results showed that the sensitivity of the electrodes still maintain 88.7 % of the initial sensitivity after 30 days storage (Fig. S8), indicating their outstanding stability and reusability.

3.4. The test in rabbit serum samples

The measurements of glucose in real samples were carried out with rabbit serum for the $Cu(OH)_2$@Au@$Co(OH)_2$ modified sensors, and compared with that measured by the commercial glucometer (ACON). As shown in Fig. 6D, upon the successive injection of serum into the reaction cell (the last four injections), the current intensity increased staircase as that measured for glucose solution (the first four injections). The glucose concentration in serum was calculated based on the response in Fig. 6D and summarized in Table S2. The results exhibited the satisfied relative standard deviation (RSD) of ≤ 7.5 % as compared with glucometer, which was less than the deviation of 20 % as regulated by the US Food and Drug Administration (FDA) for clinical blood glucose monitoring systems [59]. More clinical samples usually should be measured with sufficient batches of electrodes before carrying for any clinical applications. However, in this article, we focused more on the basis of fabrication and optimization of enzyme-mimicking nanocomposites for glucose monitoring.

4. Conclusion

In this study, a kind of hollow $Cu(OH)_2$@Au@$Co(OH)_2$ nanocomposites with controllable morphology were successfully prepared for the ultrasensitive sensing of glucose. By regulation of the etching concentrations, reaction kinetic and material components, structural nanocomposites with different surface morphologies of nanoparticles, nanowires and nanosheets were obtained. Among which, the nanoflowers structure stacked by nanowires or nanosheets possessed the highest activity for glucose catalysis, might be ascribed to the abundant paths for electron transfer from reactive center to electrode surface, and the ample electrode-electrolyte channels for OH^- permeation. Meanwhile, due to the introduction of Au nanoparticles at the interface of the core and shell layer, electron transfer rate was remarkably improved. Consequently, for the detection of glucose, the as-prepared Cu$(OH)_2$@Au@$Co(OH)_2$ showed an ultrahigh sensitivity of 3427 μA mM^{-1} cm^{-2}, as well as a wide linear range of 0.001–5.2 mM and a low detection limit of 0.5 μM. The as-prepared sensor also presented high selectivity and long-term stability, as well as high accuracy for rabbit serum measurement as compared with the commercial glucometer. We believe that this method pave a way for the preparation of the enzyme-mimicking nanocomposites, and the development of highly sensitive and stable glucose sensors in clinical applications.

CRediT authorship contribution statement

Danfeng Jiang: Conceptualization, Methodology, Investigation, Writing - original draft. **Qingwen Zhang:** Conceptualization, Methodology, Writing - review & editing. **Changshun Xu:** Visualization, Investigation, Resources. **Yuancai Ge:** Methodology, Writing - review & editing. **Liping Huang:** Visualization, Investigation, Resources. **Xueqian Ren:** Visualization, Investigation, Resources. **Yi Wang:** Conceptualization, Supervision, Project administration, Funding

acquisition, Writing - review & editing.

Declaration of Competing Interest

The authors declare that they have no known competing financial interests or personal relationships that could have appeared to influence the work reported in this paper.

Acknowledgements

This work was financially supported by National Natural Science Foundation of China (21605116), Zhejiang Province Natural Science Fund for Distinguished Young Scholars (Grant No. LR19H180001), Public Projects of Zhejiang Province (2017C33193), Science and Technology Development Project of Wenzhou Longwan's (2016YG15), Public Projects of Wenzhou (Y20160067, Y20160065, G20170011, G20170007), Leading Talent Innovation and Entrepreneurship Project of Wenzhou (RX2016005), the scientific research fund of National Health Commission (wkj-zj-1707) and Zhejiang Clinical Functional Materials and Diagnostic Devices Engineering Technology Research Center Open Fund Project (WIBEK181003).

Appendix A. Supplementary data

Supplementary material related to this article can be found, in the online version, at doi:https://doi.org/10.1016/j.snb.2020.128500.

References

[1] E. Dassau, F. Cameron, H. Lee, B.W. Bequette, H. Zisser, L. Jovanovič, H.P. Chase, D.M. Wilson, B.A. Buckingham, F.J. Doyle, Real-time hypoglycemia prediction suite using continuous glucose monitoring diabetes, Care 33 (2010) 1249–1254.
[2] X. Xuan, H.S. Yoon, J.Y. Park, A wearable electrochemical glucose sensor based on simple and low-cost fabrication supported micro-patterned reduced graphene oxide nanocomposite electrode on flexible substrate, Biosens. Bioelectron. 109 (2018) 75–82.
[3] P. Saeedi, I. Petersohn, P. Salpea, B. Malanda, S. Karuranga, N. Unwin, S. Colagiuri, L. Guariguata, A.A. Motalla, K. Ogurtsova, J.E. Shaw, D. Bright, R. Williams, Global and regional diabetes prevalence estimates for 2019 and projections for 2030 and 2045: Results from the International Diabetes Federation Diabetes Atlas, 9th edition, Diabetes Res. Cin. Pr 157 (2019) 107843.
[4] D.C. Klonoff, Continuous glucose monitoring, Diabetes Care 28 (2005) 1231–1239.
[5] S.K. Vashist, Continuous glucose monitoring systems: a review, Diagnostics 3 (2013) 385–412.
[6] D.F. Jiang, Z.Y. Chu, J.M. Peng, J.Y. Luo, Y.Y. Mao, P.Q. Yang, W.Q. Jin, One-step synthesis of three-dimensional $Co(OH)_2$/rGO nano-flowers as enzyme-mimic sensors for glucose detection, Electrochim. Acta 270 (2018) 147–155.
[7] J. Kim, A.S. Campbell, J. Wang, Wearable non-invasive epidermal glucose sensors: a review, Talanta 177 (2018) 163–170.
[8] S. Park, H. Boo, T.D. Chung, Electrochemical non-enzymatic glucose sensors, Anal. Chim. Acta 556 (2006) 46–57.
[9] K.E. Toghill, G.R. Richard, Electrochemical non-enzymatic glucose sensors: a perspective and an evaluation, Int. J. Electrochem. Sci. 5 (2010) 1246–1301.
[10] K. Li, G.L. Fan, L. Yang, F. Li, Novel ultrasensitive non-enzymatic glucose sensors based on controlled flower-like CuO hierarchical films, Sens. Actuator B Chem. 199 (2014) 175–182.
[11] Z.F. Gao, L.Q. Zhang, C. Ma, Q.D. Zhou, Y.S. Tang, Z.Q. Tu, W. Yang, L.S. Cui, Y.F. Li, TiO_2 decorated Co_3O_4 acicular nanotube arrays and its application as a non-enzymatic glucose sensor, Biosens. Bioelectron. 80 (2016) 511–518.
[12] S. Liu, B. Yu, T. Zhang, A novel non-enzymatic glucose sensor based on NiO hollow spheres, Electrochim. Acta 102 (2013) 104–107.
[13] I. Shackery, U. Patil, A. Pezeshki, N.M. Shinde, S. Kang, S. Im, S.C. Jun, Copper hydroxide nanorods decorated porous graphene foam electrodes for non-enzymatic glucose sensing, Electrochim. Acta 191 (2016) 954–961.
[14] J. Tashkhourian, S.F. Nami-Ana, M. Shamsipur, A new bifunctional nanostructure based on two-dimensional nanolayered of $Co(OH)_2$ exfoliated graphitic carbon nitride as a high performance enzyme-less glucose sensor: impedimetric and amperometric detection, Anal. Chim. Acta 1034 (2018) 63–73.
[15] X. Wu, F.L. Li, C.J. Zhao, X.Z. Qian, One-step construction of hierarchical $Ni(OH)_2$/RGO/Cu_2O on Cu foil for ultra-sensitive non-enzymatic glucose and hydrogen peroxide detection, Sens. Actuator B Chem. 274 (2018) 163–171.
[16] Z. Wang, X.Q. Cao, D.N. Liu, S.A. Hao, R.M. Kong, G. Du, A.M. Asiri, X.P. Sun, Copper nitride nanowires array: an efficient dual-functional catalyst electrode for sensitive and selective non-enzymatic glucose and hydrogen peroxide sensing, Chem.-Eur. J. 23 (2017) 4986–4989.
[17] F.Y. Xie, X.Q. Cao, F.L. Qu, A.M. Asiri, X.P. Sun, Cobalt nitride nanowire array as an efficient electrochemical sensor for glucose and H_2O_2 detection, Sens. Actuators B Chem. 255 (2018) 1254–1261.
[18] H. Wang, K.W. Wan, X.H. Shi, Recent advances in nanozyme research, Adv. Mater. 31 (2018) 1805368.
[19] J.J.X. Wu, S.R. Li, H. Wei, Multifunctional nanozymes: enzyme-like catalytic activity combined with magnetism and surface plasmon resonance, Nanoscale Horiz. 3 (2018) 367–382.
[20] T. Dayakar, K.V. Rao, K. Bikshalu, V. Malapati, K.K. Sadasivuni, Non-enzymatic sensing of glucose using screen printed electrode modified with novel synthesized CeO_2@CuO core shell nanostructure, Biosens. Bioelectron. 111 (2018) 166–173.
[21] M.H. Li, F.G. Liang, H. Zhou, F. Wu, Y. Lu, H.J. Luo, Y.X. Zhang, B.S. Hue, Three-dimensional porous MXene/NiCo-LDH composite for high performance non-enzymatic glucose sensor, Appl. Surf. Sci. 495 (2019) 143554.
[22] C.Y. Zhou, L. Xu, J. Song, R.Q. Xing, S. Xu, D.L. Liu, H.W. Song, Ultrasensitive non-enzymatic glucose sensor based on three-dimensional network of ZnO-CuO hierarchical nanocomposites by electrospinning, Sci. Rep. 4 (2014) 7382.
[23] C.C. Hou, C.J. Wang, Qi.Q. Chen, X.J. Lv, W.F. Fu, Y. Chen, Rapid synthesis of ultralong $Fe(OH)_3$:$Cu(OH)_2$ core-shell nanowires self-supported on copper foam as a highly efficient 3D electrode for water oxidation, Chem. Commun. 52 (2016) 14470–14473.
[24] L.S. Xie, C. Tang, K.Y. Wang, G. Du, A.M. Asiri, X.P. Sun, Cu(OH)2@CoCO3(OH)2·nH2O core-shell heterostructure nanowire array: an efficient 3D anodic catalyst for oxygen evolution and methanol electrooxidation, Small 13 (2017) 1602755.
[25] C.-H. Lien, C.-C. Hu, C.-T. Hsu, D.S.-H. Wong, High-performance asymmetric supercapacitor consisting of Ni-Co-Cu oxy-hydroxide nanosheets and activated carbon, Electrochem. Commun. 34 (2013) 323–326.
[26] S. Zhu, Z.D. Wang, F.Z. Huang, H. Zhang, S.K. Li, Hierarchical $Cu(OH)_2$@$Ni_2(OH)_2CO_3$ core/shell nanowire arrays in situ grown on three-dimensional copper foam for high-performance solid-state supercapacitors, J. Mater. Chem. A 5 (2017) 9960–9969.
[27] S. Fu, G.L. Fan, L. Yang, F. Li, Non-enzymatic glucose sensor based on Au nanoparticles decorated ternary Ni-Al layered double hydroxide/single-walled carbon nanotubes/graphene nanocomposite, Electrochim. Acta 152 (2015) 146–154.
[28] L. Shi, Y. Wang, S.M. Ding, Z.Y. Chu, Y. Yin, D.F. Jiang, J.Y. Luo, W.Q. Jin, A facile and green strategy for preparing newly-designed 3D graphene/gold film and its application in highly efficient electrochemical mercury assay, Biosens. Bioelectron. 89 (2017) 871–879.
[29] D.F. Jiang, J. Pang, Q.N. You, T. Liu, Z.Y. Chu, W.Q. Jin, Simultaneous biosensing of catechol and hydroquinone via a truncated cube shaped Au/PBA nanocomposite, Biosens. Bioelectron. 124–125 (2019) 260–267.
[30] C. Burda, X.B. Chen, R. Narayanan, M.A. El-Sayed, Chemistry and properties of nanocrystals of different shapes, Chem. Rev. 105 (2005) 1025.
[31] D.F. Jiang, Z.Y. Chu, J.M. Peng, W.Q. Jin, Screen-printed biosensor chips with Prussian blue nanocubes for the detection of physiological analytes, Sens. Actuators B: Chem. 228 (2016) 679–687.
[32] T. Liu, Z.Y. Chu, W.Q. Jin, Electrochemical mercury biosensors based on advanced nanomaterials, J. Mater. Chem. B 7 (2019) 3620–3632.
[33] Y. Zhao, L. Jiang, Hollow micro/nanomaterials with multilevel interior structures, Adv. Mater. 21 (2009) 3621–3638.
[34] H. Zhu, L. Li, W. Zhou, Z.P. Shao, X.J. Chen, Advances in non-enzymatic glucose sensors based on metal oxides, J. Mater. Chem. B 4 (2016) 7333–7349.
[35] Q.Q. Wang, H. Wei, Z.Q. Zhang, E.K. Wang, S.J. Dong, Nanozyme: An emerging alternative to natural enzyme for biosensing and immunoassay, Trac-Trend Anal. Chem. 105 (2018) 218–224.
[36] J. Hu, M. Chen, X. Fang, L. Wu, Fabrication and application of inorganic hollow spheres, Chem. Soc. Rev. 40 (2011) 5472–5491.
[37] J.M. Jeong, B.G. Choi, S.C. Lee, K.G. Lee, S.J. Chang, Y.K. Han, Y.B. Lee, H.U. Lee, S. Kwon, G. Lee, C.S. Lee, Y.S. Huh, Hierarchical hollow spheres of Fe_2O_3@polyaniline for lithium ion battery anodes, Adv. Mater. 25 (2013) 6250–6255.
[38] S.C. Warren, M.R. Perkins, A.M. Adams, M. Kamperman, A.A. Burns, H. Arora, E. Herz, T. Suteewong, H. Sai, Z.H. Li, J. Werner, J.H. Song, U. Werner-Zwanziger, J.W. Zwanziger, M. Grätzel, F.J. DiSalvo, U. Wiesner, A silica sol-gel design strategy for nanostructured metallic materials, Nat. Mater. 11 (2012) 460–467.
[39] W. Zhu, Z. Chen, Y. Pan, R.Y. Dai, Y. Wu, Z.B. Zhuang, D.S. Wang, Q. Peng, C. Chen, Y.D. Li, Functionalization of hollow nanomaterials for catalytic applications: nanoreactor construction, Adv. Mater. 31 (2018) 1800426.
[40] J.H. Lee, Gas sensors using hierarchical and hollow oxide nanostructures: overview, Sens. Actuator B Chem. 140 (2009) 319–336.
[41] L.F. Shen, L. Yu, H.B. Wu, X.Y. Yu, X.G. Zhang, X.W. Lou, Formation of nickel cobalt sulfide ball-in-ball hollow spheres with enhanced electrochemical pseudocapacitive properties, Nat. Commun. 6 (2015) 6694.
[42] L. Zhang, B.H. Wu, X.W. Lou, Metal-organic-frameworks-derived general formation of hollow structures with high complexity, J. Am. Chem. Soc. 135 (2013) 10664–10672.
[43] L. Han, X.-Y. Yu, X.W. Lou, Formation of prussian-blue-Analog nanocages via a direct etching method and their conversion into Ni-co-mixed oxide for enhanced oxygen evolution, Adv. Mater. 28 (2016) 4601–4605.
[44] Z.Y. Chu, Y. Liu, W.Q. Jin, Recent progress in Prussian blue films: methods used to control regular nanostructures for electrochemical biosensing applications, Biosens. Bioelectron. 96 (2017) 17–25.
[45] S.F. Xie, N. Lu, Z.X. Xie, J.G. Wang, M.J. Kim, Y.N. Xia, Synthesis of Pd-Rh core–frame concave nanocubes and their conversion to Rh cubic nanoframes by selective etching of the Pd cores, Angew. Chem. Int. Ed. 51 (2012) 1–6.
[46] H.T. Bui, D.Y. Ahn, N.K. Shrestha, M.M. Sung, J.K. Lee, S.-H. Han, Self-assembly of cobalt hexacyanoferrate crystals in 1-D array using ion exchange transformation route for enhanced electrocatalytic oxidation of alkaline and neutral water, J.

Mater. Chem. A 4 (2016) 9781–9788.
[47] X.J. Wei, Y.H. Li, H.R. Peng, D. Gao, Y.Q. Ou, Y.B. Yang, J.R. Hu, Y.H. Zhang, P. Xiao, A novel functional material of Co_3O_4/Fe_2O_3 nanocubes derived from a MOF precursor for high-performance electrochemical energy storage and conversion application, Chem. Eng. J. 355 (2019) 336–340.
[48] V. Balakumar, P. Prakash, An in-situ synthesis of novel Au@NG-PPy nanocomposite for enhanced electrocatalytic activity toward selective and sensitive sensing of catechol in natural samples, Sens. Actuators B Chem. 253 (2015) 392–399.
[49] A. Indra, U. Paik, T. Song, Boosting electrochemical water oxidation with metal hydroxide carbonate templated Prussian blue analogues, Angew. Chemie Int. Ed. English 57 (2018) 1241–1245.
[50] R. Martinez-Garcia, E. Reguera, J. Rodriguez, J. Balmaseda, J. Roque, Crystal structures of some manganese (II) and cadmium hexacyanoferrates (II, III) and structural transformations related to the sorption of Cesium, Powder Diffr. 19 (2004) 255–264.
[51] K. Castro, M.D. Rodríguez-Laso, L.A. Fernández, J.M. Madariaga, Fourier transform Raman spectroscopic study of pigments present in decorative wallpapers of the middle nineteenth century from the Santa Isabel factory (Vitoria, Basque Country, Spain), J. Raman Spectrosc. 33 (2002) 17–25.
[52] P. Salazar, M. Martín, J.L. González-Mora, A.R. González-Elipe, Application of Prussian Blue electrodes for amperometric detection of free chlorine in water samples using Flow Injection Analysis, Talanta 146 (2016) 410–416.
[53] X.L. Huang, X. Zhao, Z.L. Wang, L.M. Wang, X.B. Zhang, Facile and controllable one-pot synthesis of an ordered nanostructure of $Co(OH)_2$ nanosheets and their modification by oxidation for high-performance lithium-ion batteries, J. Mater. Chem. 22 (2012) 3764–3769.
[54] J.G. Yu, J.R. Ran, Facile preparation and enhanced photocatalytic H_2-production activity of Cu(OH)2 cluster modified TiO_2, Energy Environ. Sci. 4 (2011) 1364–1371.
[55] B. Peng, T.T. Song, T. Wang, L.Y. Chai, W.C. Yang, X.R. Li, C.F. Li, H.Y. Wang, Facile synthesis of Fe_3O_4@$Cu(OH)_2$ composites and their arsenic adsorption application, Chem. Eng. J. 299 (2016) 15–22.
[56] L. Li, H.F. Qian, J.C. Ren, CdTe@ $Co(OH)_2$ (core-shell) nanoparticles: aqueous synthesis and characterization, Chem. Commun. (J. Chem. Soc. Sect. D) 32 (2005) 4083–4085.
[57] S. Cinti, F. Arduini, D. Moscone, G. Palleschi, A.J. Killard, Development of a hydrogen peroxide sensor based on screen-printed electrodes modified with inkjet-printed Prussian blue nanoparticles, Sensors 14 (2014) 14222–14234.
[58] K.K. Lee, W.S. Chin, C.H. Sow, Cobalt-based compounds and composites as electrode materials for high-performance electrochemical capacitors, J. Mater. Chem. 2 (2014) 17212–17248.
[59] J.A. DuBois, R.J. Slingerland, M. Fokkert, Al. Roman, N.K. Tran, W. Clarke, D.A. Sartori, T.L. Palmieri, A. Malic, M.E. Lyon, A.W. Lyon, Bedside glucose monitoring-is it safe? A new, regulatory-compliant risk assessment evaluation protocol in critically ill patient care settings, Crit. Care Med. 45 (2017) 567–574.

Danfeng Jiang received his B.Sc. degree in chemical engineering from the Department of Chemistry and Chemical Engineering, Nantong University, China in 2014 and received his Ph.D. degree in chemical engineering from the Department of Chemical Engineering, Nanjing Tech University, China in 2019. He is now a research assistant professor at Wenzhou Institute, University of Chinese Academy of Sciences.

Qingwen Zhang received her B.Sc. degree in chemistry from the Department of Chemistry, Taishan University, China in 2008 and received her Ph.D. degree in physical chemistry from the Department of Chemistry and Chemical Engineering, Beijing Institute of Technology, China in 2014. She is now a research assistant professor at Wenzhou Institute, University of Chinese Academy of Sciences.

Changshun Xu received his B.Sc. degree in preventive medicine from the Department of Public Health, Zhengzhou University, China in 2018. Currently he is undertaking the master research at Wenzhou Medical University.

Yuancai Ge received his B.Sc. degree in Engineering from the School of Materials Science and Engineering, Wuhan University of Technology, China in 2014 and received his Ph.D. degree in Engineering from the Department of Materials Science, Fudan University, China in 2019. He is now a research assistant at Wenzhou Medical University.

Liping Huang received his B.Sc. degree in marine pharmacy from the Department of Food and Pharmaceutical Science, Ningbo University, China in 2018. Currently he is undertaking the master research at Wenzhou Medical University.

Xueqian Ren received her B.Sc. degree in laboratory medicine technology from the Department of Laboratory Medicine, Chongqing Medical University, China in 2018. Currently she is undertaking the master research at Wenzhou Medical University.

Yi Wang is currently a professor at Wenzhou Institute, University of Chinese Academy of Sciences, and Wenzhou Medical University. He obtained his PhD in 2010 from Max-Planck Institute for Polymer Research in Mainz, Germany. After that he worked as a research fellow at Austrian Institute of Technology, Austria and Nanyang Technological University, Singapore from 2011 to 2015. He has published over 50 peer-reviewed journal papers on nanomaterials based biosensors. His research interests include the development of plasmonic nanostructure, nanocomposites, novel polymers and peptide-functionalized materials for optical, electrical biosensors.